PHYSICAL REVIEW MATERIALS **1**, 030401(R) (2017)

Crystal growth in fluid flow: Nonlinear response effects

H. L. Peng,[1,2] D. M. Herlach,[1,2] and Th. Voigtmann[1,3]

[1]*Institut für Materialphysik im Weltraum, Deutsches Zentrum für Luft- und Raumfahrt (DLR), 51170 Köln, Germany*

[2]*Experimentalphysik IV, Ruhr-Universität Bochum, Universitätsstrasse 150, 44780 Bochum, Germany*

[3]*Department of Physics, Heinrich-Heine-Universität Düsseldorf, Universitätsstraße 1, 40225 Düsseldorf, Germany*

(Received 5 October 2016; revised manuscript received 11 June 2017; published 7 August 2017)

We investigate crystal-growth kinetics in the presence of strong shear flow in the liquid, using molecular-dynamics simulations of a binary-alloy model. Close to the equilibrium melting point, shear flow always suppresses the growth of the crystal-liquid interface. For lower temperatures, we find that the growth velocity of the crystal depends nonmonotonically on the shear rate. Slow enough flow enhances the crystal growth, due to an increased particle mobility in the liquid. Stronger flow causes a growth regime that is nearly temperature-independent, in striking contrast to what one expects from the thermodynamic and equilibrium kinetic properties of the system, which both depend strongly on temperature. We rationalize these effects of flow on crystal growth as resulting from the nonlinear response of the fluid to strong shearing forces.

DOI: 10.1103/PhysRevMaterials.1.030401

Crystallization, a paradigmatic first-order phase transformation, is of utmost importance in materials science and engineering. Many materials, for example, most polymeric and metallic materials of daily life, are produced from the liquid state as their parent phase, in the presence of strong flow (e.g., in extrusion or casting processes). Since crystal growth governs the evolution of the microstructure, detailed knowledge of how crystallization is affected by the processing conditions offers an effective way to design and control material properties in applications [1–5]. Flow effects have been studied extensively for metallic melts, and they are in particular also relevant for soft materials, where typical flow rates are of the order of typical structural relaxation times. Yet, an understanding of the microscopic principles of flow-induced changes to nucleation and crystal growth still presents a challenge to statistical physics.

Crystallization from the melt consists of two stages: nucleation of an initial crystalline seed, and subsequent growth. Despite its simplifications, classical nucleation theory (CNT) continues to be a useful reference for nucleation [6]. The effect of flow on nucleation as studied in simulation [7–11] can reasonably well be understood by accounting for the flow-induced changes in the near-equilibrium thermodynamic quantities of CNT [12–15].

Crystal growth on the other hand needs to be discussed as a nonequilibrium process that is strongly influenced by external driving forces [16]. Once an initial crystal has formed, in a sheared liquid crystal growth and flow-induced erosion compete and lead to a nonequilibrium coexistence that depends on temperature and flow rate [17]. It has already been emphasized that a near-equilibrium thermodynamic description of flow-modified growth kinetics is not viable [17–19]. It is therefore much less clear, how crystal growth changes under strong fluid flow, and which are the governing microscopic processes.

Here we present molecular-dynamics (MD) simulations of crystal growth in a homogeneously sheared fluid, over a wide range of temperatures and shear rates. We argue that the nonlinear response of the fluid to the shearing force is a relevant microscopic dynamical process that determines a set of qualitatively different growth regimes. Strikingly, we find that the growth velocity of the crystal in a deeply undercooled fluid is a nonmonotonic function of the shear rate. After an initial strongly temperature-dependent increase, a regime of intermediate shear rates appears where the crystal grows with a velocity that is nearly temperature independent. It is rationalized as the result of strong shear thinning of the undercooled fluid. This nonlinear-response effect has so far, to our knowledge, been neglected in the modeling of solidification processes. It is achieved once shear-induced "surface erosion" and structural relaxation of the viscoelastic melt compete. This regime of flow rates is of particular relevance for soft materials, but can in principle also be reached for sufficiently undercooled metallic melts.

We performed molecular-dynamics (MD) simulations of a binary mixture that crystallizes into a B_2 structure (CsCl lattice). To provide a specific reference point, we use an embedded-atom model of the intermetallic compound $Al_{50}Ni_{50}$ [20], a material that is used in many applications, e.g., for turbines in aeroplanes or power stations. $Al_{50}Ni_{50}$ melts congruently, so that crystal growth can be studied without any constitutional effects. The model has also been extensively studied in previous MD simulations, investigating its liquid dynamics [21], glass-forming ability [22], quiescent crystal growth [22–24], and disorder trapping [25]. Using $N = 27040$ particles in a box of average dimensions $L_x : L_y : L_z = 1 : 1 : 6.4$ and $L_x \approx 38$ Å (employing periodic boundary conditions in all Cartesian directions), seeded with an initial crystal that is surrounded by liquid regions, we study crystal growth along the normal of the (100) face (along the z direction). The system is first prepared in its B_2 state and relaxed to the target temperature. Next, particles in the central third of the box ($L_z/3 \approx 81$ Å) are fixed, and the surrounding system is molten at $T = 3000$ K before it is brought to the desired temperature again.

Simple shear flow parallel to the interface is imposed by assigning a fixed center-of-mass velocity to small fluid layers (width 12 Å) at the z boundaries of the simulation box, while keeping a layer of 10 Å fixed in the crystalline center. After an initial transient (of about 100 ps), a homogeneous linear velocity profile develops in the liquid, as shown in Fig. 1. The shear rate, $\dot{\gamma}$, is extracted from the averaged velocity,

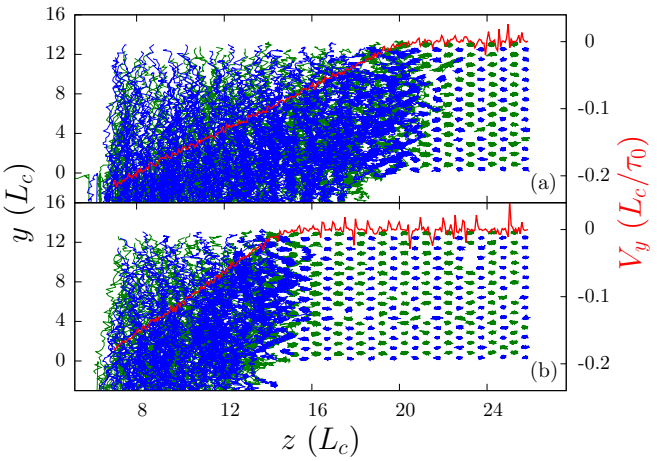

FIG. 1. Snapshots of the simulation of crystal growth along the z direction, in a fluid sheared in the y-z plane, for two different times. Units are fixed by the microscopic relaxation time τ_0 and the lattice constant L_c ($\tau_0 = 0.2$ ps and $L_c = 2.897$ Å for Al-Ni [20]). Blue and green lines indicate the positions of Ni and Al atoms, respectively, over a small time window. Red lines indicate the average velocity of the atoms along the z direction, highlighting the development of a homogeneous linear shear profile in the fluid region.

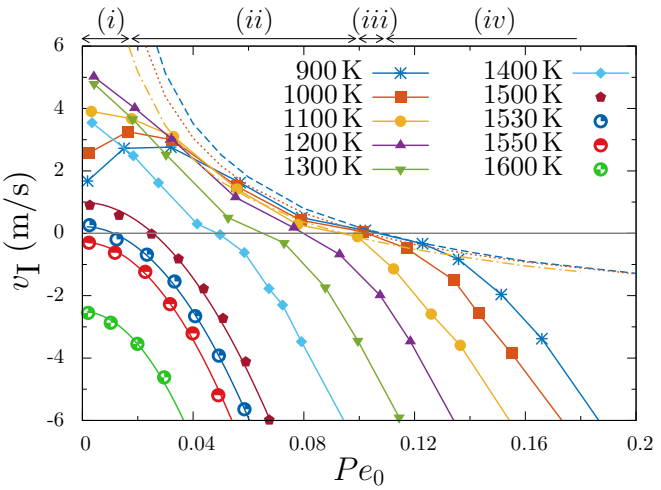

FIG. 2. Crystal-fluid interface velocity v_I as a function of shear rate $Pe_0 = \dot{\gamma}\tau_0$ for different temperatures T as labeled. Labels (i) to (iv) indicate for $T = 900$ K the different growth regimes discussed in the text. Dashed lines are estimates from Eq. (2) for $T \leqslant 1100$ K.

$\dot{\gamma} = \partial_z v_y$. Data are analyzed in small time windows during which the shear rate does not change appreciably. To release latent heat as the crystal grows, we employ a profile-unbiased thermostat [26] in slabs (of width 4 Å) parallel to the interface [27]. A barostat along the growth direction keeps $p_z = 0$ and compensates for the volume expansion during the crystallization process.

The time-dependent crystal-liquid interface position z_I is obtained from both the local fluid velocity, as the point where $|v_y(z_I)| < 0.05$ Å/ps, and from the crystalline order-parameter field, $\Psi(z)$, as the point where $\Psi(z_I) > 0.01$. Here, $\Psi(z)$ measures four-fold symmetry in the plane perpendicular to the growth direction:

$$\Psi(z) = \left\langle \sum_i \delta(z_i - z) \frac{1}{M(M-1)} \sum_{j \neq k} \cos(8\theta_{ijk}) \right\rangle, \qquad (1)$$

where the sums over j and k extend over the nearest-neighbor atoms of particle i (defined as those M atoms whose relative distance is less than that of the first minimum in the liquid-state pair distribution function), and θ_{ijk} is the angle in the x-y plane between the distance vectors $\vec{r}_{ij}$ and $\vec{r}_{ik}$. The interface positions obtained by both methods differ by about 5 Å, indicating a hydrodynamic slip length, but give consistent growth velocities.

The temperature- and shear-rate dependent growth velocity $v_I(T;\dot{\gamma})$ of the crystal is shown in Fig. 2 as a function of shear rate $\dot{\gamma}$. Here and in the following, we use the time scale of atomic vibrations, $\tau_0 \approx 0.2$ ps to define a dimensionless shear rate,[1] the (bare) Péclet number $Pe_0 = \dot{\gamma}\tau_0$. We briefly remark on the behavior close to the equilibrium melting temperature ($T_m \approx 1540$ K in our model). Here, shear flow always suppresses crystal growth, and the growth velocities v_I closely follow a quadratic dependence on $\dot{\gamma}$. The zeros of the v_I-versus-$\dot{\gamma}$ curves identify a nonequilibrium crystal-fluid coexistence [at a shear rate $\dot{\gamma}_{\rm coex}(T)$] that has been discussed earlier [17–19]. Crystal growth velocities close to T_m are usually expressed in terms of thermodynamic free-energy barriers, and it is tempting to relate the quadratic decrease of v_I to a shifted effective chemical-potential difference between the liquid and the crystal (and hence to a process-dependent effective undercooling [28]). However, the shear-induced change in the strained crystal's free energy is much too small to quantitatively explain the simulation data [18].

For deeper undercooling, in particular, the situation is far more complex: the growth rate displays a nonmonotonic dependence on the shear rate at any fixed temperature, with a maximum at a nonzero intermediate rate, and an inflection point around $\dot{\gamma}_{\rm coex}$. Between the maximum and the coexistence point, the temperature dependence of the growth rate is remarkably weak, i.e., the interface velocity is described well by a temperature-independent master curve $v_I(\dot{\gamma})$ in an intermediate shear-rate regime. This is unexpected from the point of view of thermodynamics (where Boltzmann factors imply a temperature dependence when keeping other parameters fixed), or from the strong slowing down of the transport kinetics in the fluid that occurs upon cooling.

To understand the mechanisms responsible for the nonmonotonic dependence of the growth velocity on the shear rate, let us divide the v_I-versus-$\dot{\gamma}$ curves into four regimes, as labeled in Fig. 2: (i) for slow shear, the suppression of growth due to shear that is observed close to T_m, changes to an enhancement below some temperature ($T \approx 1000$ K

[1]The time scales of single-particle vibrations, τ_0, and that of collective structural relaxation, τ, have been determined from the intermediate scattering functions in the quiescent fluid, at wave vectors corresponding to typical interparticle distances.

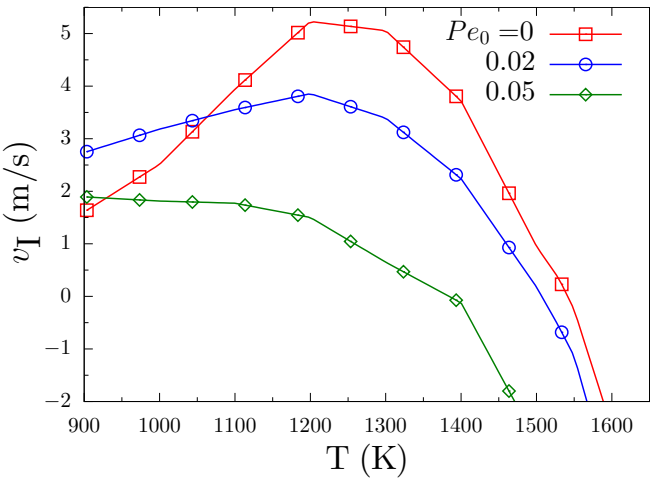

FIG. 3. Interface velocity v_I as a function of temperature T, for constant shear rates given by bare Péclet numbers $Pe_0 = \dot{\gamma}\tau_0 = 0$ (squares), 0.02 (circles), and 0.05 (diamonds).

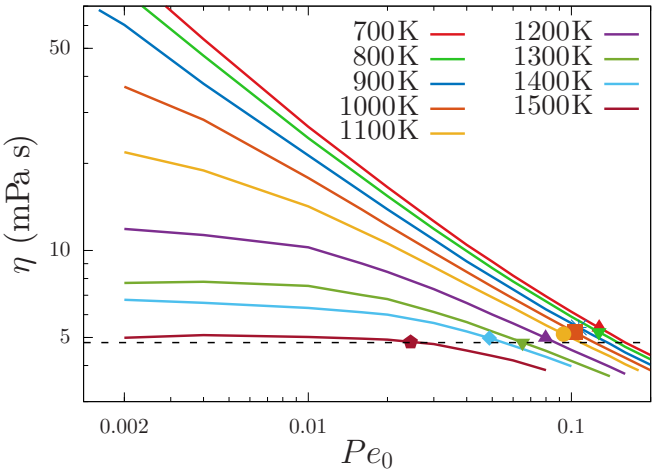

FIG. 4. Bulk fluid viscosity $\eta(\dot{\gamma})$ as a function of shear rate, $Pe_0 = \dot{\gamma}\tau_0$. Symbols mark the points where for each temperature, $\dot{\gamma} = \dot{\gamma}_{\rm coex}$, i.e., the points where $v_I = 0$. A horizontal dashed line indicates the equilibrium melting-point viscosity η_m.

in the figure). (ii) At intermediate shear rates, v_I decreases towards zero with increasing $\dot{\gamma}$. The curves for $T \lesssim 1200$ K approach a T-independent master curve for $0.03 \lesssim Pe_0 \lesssim 0.1$ (0.15 ps$^{-1} \lesssim \dot{\gamma} \lesssim 0.5$ ps^{-1}). The interplay between (i) and (ii) causes the maximum in the growth velocity for a finite shear rate, visible at the lowest temperatures shown in Fig. 2(a). (iii) The coexistence regime around $v_I(\dot{\gamma}_{\rm coex}) = 0$ becomes broader in the sense that the depedence of the growth velocity on shear rate becomes weak, i.e., near-stationarity of the interface is achieved for a wider range of shear rates. (iv) At larger shear rates, the crystal shrinks again.

For the explanation of regime (i) of Fig. 2, recall that the undercooled liquid dynamics is characterized by slow structural relaxation: density fluctuations decay on a time scale $\tau \gg \tau_0$. With decreasing temperature, τ increases much more rapidly than expected from the high-temperature Arrhenius behavior. Hence the mobility of atoms in the liquid drops sharply, and the crystal-growth mechanism in the quiescent liquid changes from thermodynamically limited around T_m to kinetically limited at $T \ll T_m$. As shown in Fig. 3, the resulting growth velocity $v_I(T; \dot{\gamma} = 0)$ exhibits a maximum as a function of temperature (around $T = 1200$ K in our simulation) [22,29].

Structural relaxation speeds up in the sheared fluid when the (dressed) Péclet number $Pe = \dot{\gamma}\tau$ is of the order of the strain required to break typical nearest-neighbor cages, $\gamma_c \approx 10\%$. This is a well-known nonlinear-response effect in metallic melts [30] and most viscoelastic fluids [31] that gives rise to shear thinning—a pronounced decrease in the fluid's shear viscosity with increasing shear rate, as shown in Fig. 4 for our system. All data shown in Fig. 2 for $T \lesssim 1100$ K correspond to $Pe \gtrsim \gamma_c$. As a result, particle mobility in the fluid is enhanced by the flow, and the growth velocity v_I increases with increasing $\dot{\gamma}$ initially for those T where the equilibrium growth is limited kinetically.

Regime (ii) is essentially T-independent; this is clearly seen in Fig. 3, where the curve for $Pe_0 = 0.05$ approaches a constant for low temperatures. As opposed to regime (i), $v_I(\dot{\gamma})$ now decreases with increasing shear rate, which indicates that a qualitatively different process limits the growth. Hydrodynamic momentum transport across the interface region is governed by the rate $r_+ \sim \eta/L^2\rho$, where ρ is the fluid mass density and L the interface width ($L \approx 10$ Å in our simulations for all state points). Note that at T_m, one gets $r_+ \approx 1/\tau_0$, the natural scale for the rate of momentum transport in the crystal. Assuming that the rate r_+ limits the attachment of atoms to the interface and hence the growth, and that it balances the detachment rate at the nonequilibrium coexistence point, we get

$$v_I(\dot{\gamma}) \sim v_0 \cdot (\eta(\dot{\gamma}) - \eta(\dot{\gamma}_{\rm coex}))\,\tau_0/L^2\rho, \qquad (2)$$

where v_0 is a velocity scale set by the thermodynamic features of the system ($v_0 = \mathcal{O}(1$ m/s) in our simulation). In Eq. (2), we have accounted for the fact that the viscosity $\eta(\dot{\gamma})$ depends sensitively on the shear rate in the shear-thinning regime (ii). At the same time, structural relaxation in the fluid becomes nearly T-independent, since it is dominated by shear and thus $1/\dot{\gamma}$ is the only relevant time scale. The fluid then flows plastically, i.e., at the expense of a nearly constant yield stress σ_y. As a result, also the shear viscosity $\eta(\dot{\gamma})$ entering Eq. (2) is nearly temperature-independent. Expression (2) is shown for the lowest three temperatures in Fig. 2 (dashed lines), evaluated using the viscosity of the bulk fluid (see below). It gives a reasonable qualitative account for $v_I(\dot{\gamma})$ in the range $0.04 \lesssim Pe_0 \lesssim 0.1$. For comparison, a thermodynamic argument based on an effective free-energy barrier would not account for the weak T dependence we observe. Equation (2) naturally explains that in regime (ii), the growth velocity decreases with increasing shear rate: for true yield-stress flow, $\eta(\dot{\gamma}) \sim \sigma_y/\dot{\gamma}$, and thus $v_I \sim 1/\dot{\gamma}$ up to a constant and weakly dependent on temperature.

Equation (2) implies that the fluid viscosity determines the nonequilibrium coexistence between the sheared liquid and the crystal, region (iii). To corroborate this argument, we show in Fig. 4 the shear-rate dependent viscosity of the bulk liquid, as determined from separate MD simulations (in a system of

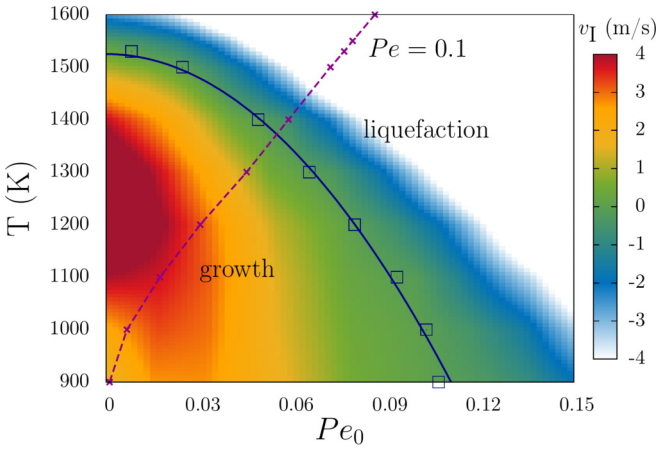

FIG. 5. Nonequilibrium crystallization diagram for the sheared $Al_{50}Ni_{50}$ fluid and B_2 crystal in the temperature–shear-rate plane. Colors indicate the growth velocity as labeled. The red line is a quadratic fit for the coexistence line. The dashed line indicates the cross-over from linear response to shear (left) to the regime of nonlinear-response flow (right).

$N = 5000$ particles following the SLLOD equations of motion [26]). Despite the fact that the bulk-liquid viscosity drops by more than an order of magnitude over the range of shear rates we investigate, the viscosity at the coexistence point (marked by symbols in Fig. 4) only varies by about 20% around the equilibrium melting-point viscosity η_m. Thus

$$\eta(\dot{\gamma}_{\rm coex}) \approx \eta_m. \tag{3}$$

This implies that in regime (iii), the dependence of $v_I(\dot{\gamma})$ on the flow rate is weak, as indeed observed in Fig. 2 for $T \lesssim 1100$ K. It indicates a rate-controlled nonequilibrium coexistence that is attributed to the non-Newtonian fluid behavior, and that is different from a thermodynamical balance.

A coexistence point is intuitively expected since shear-induced erosion of particles from the interface eventually becomes strong enough to suppress any attachment. In agreement with earlier simulations [17] and a recent model [32], a nonequilibrium phase diagram is obtained in the T-$\dot{\gamma}$ plane, shown in Fig. 5. A quadratic fit (red line in Fig. 5), gives a good description of $T_{\rm coex}(\dot{\gamma}^2)$, extrapolating to $T_{\rm coex}(0) \approx 1531$ K in reasonable agreement with the value of T_m reported for the model before [23]. The surface-erosion picture is consistent with a weak $\dot{\gamma}$ dependence of v_I close to $\dot{\gamma}_{\rm coex}$: as long as shear-induced changes in the thermodynamic forces are negligible, any fast enough shear rate will be sufficient to erode fluctuations in the interface.

Only in regime (iv), effective thermodynamic forces again dominate the crystallization process; they always lead to shear-induced melting of the crystal. To the strongly sheared liquid, an increased effective temperature $T_{\rm eff}(\dot{\gamma}) \geqslant T$ can be assigned [33], leading to a reduced effective undercooling that controls the growth velocity. Indeed, our data in regime (iv) closely follows a single η-dependent curve, where the viscosity is a proxy for the fluid's effective temperature.

In conclusion, the growth velocity of a crystal is a nonmonotonic function of the shear rate at fixed temperature. Flow initially enhances crystal growth at sufficiently strong undercooling, due to the enhanced particle mobility in the fluid. In the presence of stronger flow, the hydrodynamics of surface erosion causes a decrease in the growth velocity as a function of shear rate that is insensitive to temperature. This nonmonotonic dependence is rationalized as the result of the pronounced nonlinear-response behavior of the non-Newtonian undercooled fluid.

The strain supported by nearest-neighbor cages marks the cross-over from the regime of small shear rates to the nonlinear-response dominated regime. This cross-over is reached once the dressed Péclet number (formed with the structural-relaxation time rather than the timescale of atomic vibrations) reaches $Pe \approx 0.1$. The line corresponding to $Pe = 0.1$ is shown in Fig. 5 (dashed line).

The mechanism we propose is very generic since it rests solely on the fact that the liquid becomes shear thinning. This is the case for most undercooled (viscoelastic) fluids, including colloidal suspensions, soft materials, as well as metallic melts. Our results point out that nonlinear-response effects in the undercooled fluid likely should be taken into account in effective coarse-grained models of rapid solidification [34–36]. It is difficult to assess the actual shear rates in experiments on metallic melts. Still, an enhancement of crystal growth by (convective) flow has been reported in experiments combining high-speed imaging, electromagnetic levitation and microgravity conditions [28,37,38] to determine crystal growth velocities of alloys in the presence of convective flow on a mesoscopic scale. For the change in microscopic growth kinetics that occurs at $Pe \approx 0.1$, the relevant shear rate is a local velocity gradient in front of the interface, extending over about five to ten atomic layers in our model. Local fluid flow velocities can be in excess of tens of m/s, indicating that the nonlinear regime to right of the crossover curve in Fig. 5 might be reached in melts that can be undercooled sufficiently far.

The temperature-independent growth regime in particular is a signature of plastic yield-stress flow. It suggests the use of controlled-flow conditions in applications where the speed of crystallization needs to be adjusted separately from thermal control. We expect this mechanism to apply also to more complex systems and geometries, for example, in the presence of concentration gradients [39]. In fact, $Al_{50}Ni_{50}$ is already an example where the quiescent growth mechanism is an intricate combination of attachment and intra-layer delayed reorganization [24]. Although we observe disorder trapping at the highest growth velocities, similar to the quiescent case at strong undercooling [25,40], such details appear to leave the qualitative appearance of the different growth regimes as a function of shear rate unchanged. Our findings will be essential to further explore unusual growth kinetics observed in metallic materials, e.g., in Al-rich Al-Ni alloys where the growth velocity decreases with increasing driving force and in the presence of forced convection [41].

We acknowledge funding from Deutsche Forschungsgemeinschaft (DFG) through grant He 1601/26. We thank Peter Harrowell, Jürgen Horbach, and Jianrong Gao for discussions and valuable comments, and Jürgen Brillo for a careful reading of the manuscript.

[1] D. M. Herlach, P. K. Galenko, and D. Holland-Moritz, *Metastable Solids from Undercooled Melts* (Elsevier, Amsterdam, 2007).
[2] K. F. Kelton and A. L. Greer, *Nucleation in Condensed Matter: Applications in Materials and Biology* (Elsevier, Amsterdam, 2010).
[3] Z. Yan, K. Song, Y. Hu, F. Dai, Z. Chu, and J. Eckert, Sci. Rep. **6**, 19358 (2016).
[4] Y. Diao, Y. Zhou, T. Kurosawa, L. Shaw, C. Wang, S. Park, Y. Guo, J. A. Reinspach, K. Gu, X. Gu, B. C. K. Tee, C. Pang, H. Yan, D. Zhao, M. F. Toney, S. C. B. Mannsfeld, and Z. Bao, Nat. Commun. **6**, 7955 (2015).
[5] M. Anwar, J. T. Berryman, and T. Schilling, J. Chem. Phys. **141**, 124910 (2014).
[6] J. Bokeloh, R. E. Rozas, J. Horbach, and G. Wilde, Phys. Rev. Lett. **107**, 145701 (2011).
[7] D. Richard and T. Speck, Sci. Rep. **5**, 14610 (2015).
[8] Y. L. Wu, Proc. Natl. Acad. Sci. USA **106**, 10564 (2009).
[9] J. J. Cerdà, T. Sintes, C. Holm, C. M. Sorensen, and A. Chakrabarti, Phys. Rev. E **78**, 031403 (2008).
[10] A. V. Mokshin and J.-L. Barrat, Phys. Rev. E **77**, 021505 (2008).
[11] Z. Shao, J. P. Singer, Y. Liu, Z. Liu, H. Li, M. Gopinadhan, C. S. O'Hern, J. Schroers, and C. O. Osuji, Phys. Rev. E **91**, 020301(R) (2015).
[12] R. Blaak, S. Auer, D. Frenkel, and H. Löwen, Phys. Rev. Lett. **93**, 068303 (2004).
[13] A. V. Mokshin, B. N. Galimzyanov, and J.-L. Barrat, Phys. Rev. E **87**, 062307 (2013).
[14] F. Mura and A. Zaccone, Phys. Rev. E **93**, 042803 (2016).
[15] B. Lander, U. Seifert, and T. Speck, J. Chem. Phys. **138**, 224907 (2013).
[16] S. Dorosz, Th. Voigtmann, and T. Schilling, Europhys. Lett. **113**, 10004 (2016).
[17] S. Butler and P. Harrowell, Nature (London) **415**, 1008 (2002).
[18] S. Butler and P. Harrowell, J. Chem. Phys. **118**, 4115 (2003).
[19] S. Butler and P. Harrowell, Phys. Rev. E **67**, 051503 (2003).
[20] Y. Mishin, M. J. Mehl, and D. A. Papaconstantopoulos, Phys. Rev. B **65**, 224114 (2002).
[21] S. K. Das, J. Horbach, M. M. Koza, S. M. Chatoth, and A. Meyer, Appl. Phys. Lett. **86**, 011918 (2005).
[22] C. Tang and P. Harrowell, Nat. Mater. **12**, 507 (2013).
[23] A. Kerrache, J. Horbach, and K. Binder, Europhys. Lett. **81**, 58001 (2008).
[24] P. Kuhn and J. Horbach, Phys. Rev. B **87**, 014105 (2013).
[25] X. Q. Zheng, Y. Yang, Y. F. Gao, J. J. Hoyt, M. Asta, and D. Y. Sun, Phys. Rev. E **85**, 041601 (2012).
[26] D. J. Evans and G. P. Morriss, *Statistical Mechanics of Nonequilibrium Liquids*, 2nd ed. (Cambridge University Press, Cambridge, UK, 2008).
[27] J. Monk, Y. Yang, M. I. Mendelev, M. Asta, J. J. Hoyt, and D. Y. Sun, Modell. Simul. Mater. Sci. Eng. **18**, 015004 (2010).
[28] D. M. Herlach, Metals **4**, 196 (2014).
[29] H. Wang, D. M. Herlach, and R. P. Liu, Europhys. Lett. **105**, 36001 (2014).
[30] P. Guan, M. Chen, and T. Egami, Phys. Rev. Lett. **104**, 205701 (2010).
[31] Th. Voigtmann, Curr. Opin. Colloid Interf. Sci. **19**, 549 (2014).
[32] M. Ramsay and P. Harrowell, Phys. Rev. E **93**, 042608 (2016).
[33] L. Berthier and J.-L. Barrat, Phys. Rev. Lett. **89**, 095702 (2002).
[34] J. Lee, D. M. Matson, S. Binder, M. Kolbe, D. Herlach, and R. W. Hyers, Metall. Mater. Trans. B **45**, 1018 (2014).
[35] N. Shevchenko, O. Roshchupkina, O. Sokolova, and S. Eckert, J. Cryst. Growth **417**, 1 (2015).
[36] R. Rojas, T. Takaki, and M. Ohno, J. Comput. Phys. **298**, 29 (2015).
[37] S. Reutzel, H. Hartmann, P. K. Galenko, S. Schneider, and D. M. Herlach, Appl. Phys. Lett. **91**, 041913 (2007).
[38] S. Binder, P. K. Galenko, and D. M. Herlach, J. Appl. Phys. **115**, 053511 (2014).
[39] Y. Yang, H. Humadi, D. Buta, B. B. Laird, D. Sun, J. J. Hoyt, and M. Asta, Phys. Rev. Lett. **107**, 025505 (2011).
[40] H. Hartmann, D. Holland-Moritz, P. K. Galenko, and D. M. Herlach, Europhys. Lett. **87**, 40007 (2009).
[41] R. Lengsdorf, D. Holland-Moritz, and D. M. Herlach, Scr. Mater. **62**, 365 (2010).